Molecular Neurobiology (2019) 56:5934–5949
https://doi.org/10.1007/s12035-018-1466-1

Altered Nup153 Expression Impairs the Function of Cultured Hippocampal Neural Stem Cells Isolated from a Mouse Model of Alzheimer's Disease

Lucia Leone[1,2] · Claudia Colussi[3] · Katia Gironi[1] · Valentina Longo[1] · Salvatore Fusco[1,2] · Domenica Donatella Li Puma[1,2] · Marcello D'Ascenzo[1,2] · Claudio Grassi[1,2]

Received: 2 September 2018 / Accepted: 20 December 2018 / Published online: 28 January 2019

Abstract

Impairment of adult hippocampal neurogenesis is an early event in Alzheimer's disease (AD), playing a crucial role in cognitive dysfunction associated with this pathology. However, the mechanisms underlying defective neurogenesis in AD are still unclear. Recently, the nucleoporin Nup153 has been described as a new epigenetic determinant of adult neural stem cell (NSC) maintenance and fate. Here we investigated whether Nup153 dysfunction could affect the plasticity of NSCs in AD. Nup153 expression was strongly reduced in AD-NSCs, as well as its interaction with the transcription factor Sox2, a master regulator of NSC stemness and their neuronal differentiation. Similar Nup153 reduction was also observed in WT-NSCs treated with amyloid-β (Aβ) or stimulated with a nitric oxide donor. Accordingly, AD-NSCs treated with either a γ-secretase inhibitor or antioxidant compounds showed higher Nup153 levels suggesting that both nitrosative stress and Aβ accumulation affect Nup153 expression. Of note, restoration of Nup153 levels in AD-NSCs promoted their proliferation, as assessed by BrdU incorporation, neurosphere assay, and stemness gene expression analysis. Nup153 overexpression also recovered AD-NSC response to differentiation, increasing the expression of pro-neuronal genes, the percentage of cells positive for neuronal markers, and the acquisition of a more mature neuronal phenotype. Electrophysiological recordings revealed that neurons differentiated from Nup153-transfected AD-NSCs displayed higher Na^+ current density, comparable to those deriving from WT-NSCs. Our data uncover a novel role for Nup153 in NSCs from animal model of AD and point to Nup153 as potential target to restore physiological NSC behavior and fate in neurodegenerative diseases.

Keywords Nup153 · Neural stem cells · Nitric oxide · Adult hippocampal neurogenesis · Alzheimer's disease · Personalized medicine

Background

In the adult mammalian brain, neurogenesis mainly occurs in two specific niches, the subventricular zone and the subgranular zone (SGZ) of the dentate gyrus (DG) of the hippocampus, where the residing neural stem cells (NSCs) throughout life proliferate and differentiate into new functional neurons, thereby contributing to learning and memory [1, 2]. Decline of adult neurogenesis occurs with age and in age-related neurodegenerative diseases such as Alzheimer's disease (AD), a form of dementia featured by a massive and progressive hippocampal neuronal loss leading to cognitive deterioration and memory dysfunction [3].

A large body of evidence suggests that cognitive deficits in AD rely, at least in part, on impairment in adult neurogenesis. Indeed, reduced neurogenesis occurs in both patients and animal models of AD [4, 5] and is now considered an early event

Lucia Leone and Claudia Colussi contributed equally to this work.

Electronic supplementary material The online version of this article (https://doi.org/10.1007/s12035-018-1466-1) contains supplementary material, which is available to authorized users.

✉ Claudia Colussi
claudia.colussi@cnr.it

[1] Institute of Human Physiology, Università Cattolica del Sacro Cuore, Roma, Italia

[2] Fondazione Policlinico Universitario A. Gemelli IRCCS, Roma, Italia

[3] Institute of Cell Biology and Neurobiology, National Research Council, Largo F. Vito 1, 00168 Rome, Italy

in this pathology, although the underlying molecular mechanisms are still largely unknown. It is now accepted that both familial and sporadic forms of AD are the consequence of complex interactions of multiple risk factors, including genetic and epigenetic ones.

Epigenetic mechanisms integrate different environmental factors of the neurogenic niche to regulate NSC function. Specifically, the interaction of transcription factors and co-repressors/activators is crucial to change chromatin structure and to promote different gene expression patterns that orchestrate NSC self-renewal, proliferation, and differentiation [6]. Thus, epigenetic alterations may greatly affect adult neurogenesis and be implicated in AD etiology.

Recently, nucleoporins (Nups), which form channels in the nuclear envelope, have emerged as novel epigenetic regulators. In addition to their canonical role in nucleus-cytoplasm trafficking, several Nups are also involved in different physiological processes including development and differentiation, providing a dynamic platform for many epigenetic mechanisms [7]. Accordingly, recent evidence, including ours, indicates that Nup153 regulates gene expression by interaction with chromatin remodeling enzymes [8–10] in different pathological contexts. Remarkably, Nup153 has been reported as a regulator of embryonic stem cell pluripotency [11] and adult neural progenitor stemness maintenance and plasticity through the interaction with the transcription factor Sox2 [12]. To date, no data are available on the contribution of Nup153 to altered neurogenesis in AD, neither its possible role as therapeutic target. Of note, emerging evidence also suggests the involvement of Nups in aging [13], a condition known to be a major risk factor for AD-related cognitive decline.

Nitric oxide (•NO) signaling pathway is implicated in a variety of physiological processes including neural development, adult neural plasticity, neural progenitor migration, and differentiation [14, 15]. Indeed, the neurovascular unit is an integral part of the NSC niche [16] since it provides oxygen and nutrients as well as important signaling including •NO release in response to stimuli. Of note, age-related neurodegenerative diseases are characterized by dysregulation of the •NO pathway with overproduction of reactive oxygen (ROS), nitrogen (RNS) species and unbalance in antioxidant systems [17]. Recent evidence indicates that accumulation of amyloid-β protein (Aβ), which occurs also in glial progenitor cells [18] isolated from the APP23 AD mouse model and AD patients, affects directly or indirectly mitochondrial function thus contributing, at least in part, to the generation of oxidative/nitrosative stress occurring in AD [19].

Previous works, including ours, have shown that the pleiotropic effect of •NO is mediated by its epigenetic action and the ability to modulate the function of key chromatin remodelers [20, 21]. Recently, we described that Nup153 is an epigenetic mediator of •NO signaling controlling co-regulator complexes formation, activation, and chromatin binding [9, 22]. Accordingly, several reports described that •NO oxidative stress balance regulates Nup153 protein levels by inducing either its degradation or accumulation depending on the cellular context [23, 24].

Although the contribution of oxidative/nitrosative stress to the development of AD is well recognized [17], less known is whether it may affect neurogenesis through the impairment of epigenetic effectors such as Nup153. In the present paper, we demonstrate that nitrosative stress and Aβ accumulation affected the biological properties of AD-NSCs causing reduced levels of Nup153, a master epigenetic regulator of NSCs. Of note, rescue of Nup153 level in AD-NSCs promoted their proliferation and migration and, upon induction of differentiation, ameliorated their neuronal maturation. Our data provide evidence about the role of Nup153 as master epigenetic determinant and potential target to ameliorate AD-NSC function.

Materials and Methods

Animal Model

3×Tg-AD (*B6;129-Psen* ^{tm1Mpm}*Tg/APPSwe, tauP301L/1Lfa/Mmjax*) mice were used as AD animal model and compared with WT control mice (*B6129SF2/J*). Both adult (2 months old; WT and 3×Tg $n = 16$ each) or newborn mice (50 litters (5–6 pups per litter) WT and 3×Tg) were used in the study. When possible, the same litter was used for different types of experiments. Mice were used in agreement with the European and National guidelines as stated in the specific section "Compliance with Ethical Standards."

Neural Stem Cell Cultures

Postnatal hippocampal NSCs were isolated and cultured according to previously published protocols. Briefly, brains of newborn (0–1 day old) WT and 3×Tg mice were microdissected to obtain the hippocampal regions. Tissues were finely minced and digested by accutase (in DPBS, 0.5 mM EDTA; Innovative Cell Technologies, Inc., San Diego, CA, USA) at 37 °C for 30 min. After centrifugation, cells were carefully dissociated by passaging in fire-polished Pasteur pipettes and resuspended in Neurobasal-A medium, supplemented with 2% B27 without vitamin A (Gibco, Grand Island, NY, USA), Glutamax (0.5 mM; Invitrogen, Carlsbad, CA), mouse fibroblast growth factor 2 (FGF2, 10 ng/mL; Invitrogen), epidermal growth factor (EGF, 10 ng/mL; Invitrogen), and mouse platelet-derived growth factor bb (PDGFbb, 10 ng/mL; Invitrogen).

Cells were seeded onto 25-cm^2 T-flask and incubated at 37 °C in 5% CO_2 atmosphere. During the first week of in vitro culture, NSCs began to form neurospheres. At 2-day

intervals, neurospheres were collected and passaged by a gently enzymatic and mechanical dissociation.

To obtain monolayer cultures, neurospheres of established cultures were passaged by enzymatic and mechanical dissociation and plated as single cells onto Matrigel Matrix (Becton Dickinson, Franklin Lakes, NJ) pre-coated Petri dishes. NSCs cultured in the medium described above remained in an undifferentiated state and proliferated. To induce differentiation, NSCs were cultured in Neurobasal-A medium, for the times indicated in the legend, supplemented by 2% B27, Glutamax (0.5 mM), and 1% fetal calf serum (FCS). For electrophysiological recordings, NSCs were cultured for 48 h in differentiation medium, as described above, and then medium was changed with NeuroCult basal medium complemented with NeuroCult differentiation supplement (StemCell Technologies, Inc., Vancouver, Canada) until assay at D14.

RT-qPCR Experiments

All reverse transcription-quantitative PCR (RT-qPCR) experiments were performed as previously described with minor modifications [25].

Briefly, total RNA was extracted using an RNAqueous Micro Kit (Ambion Inc., Austin, TX, USA) according to the manufacturer's instructions. Equal amounts of RNA (2 μg) were subsequently reverse-transcribed using a high-capacity cDNA reverse transcription kit (Applied Biosystems, Foster City, CA, USA). Quantitative RT-PCR was performed in triplicates using inventoried TaqMan Gene expression assays purchased from Applied Biosystems. Relative mRNA levels for genes of interest were normalized to TATA-box-binding protein (TBP), taken as housekeeping gene, and calculated by using the $2^{-\Delta\Delta Ct}$ method. Three independent experiments were performed with the ABI 7500 Sequence Detection System Analyzer for RT-qPCR (Applied Biosystems). Results were expressed as mean fold changes induced by treatments compared with control samples. ID codes for TaqMan probes against targets analyzed in this work are provided in Table 1.

Cell Treatments

NSCs isolated from WT and 3×Tg-AD mice were treated with the following drugs: the ˙NO synthase pan-inhibitor L-NG-nitro-arginine methyl ester (LNAME-Sigma-Aldrich, 5 mM, 72 h); the ˙NO donor DETANO (Sigma-Aldrich, 100 μM for 24 h), the γ-secretase inhibitor (GSI, InSolution™ γ-Secretase Inhibitor IX–Calbiochem 1 μM, 48 h); the antioxidant compounds *N*-acetylcysteine (NAC, Sigma-Aldrich, 5 mM, 72 h) and ascorbic acid (Sigma-Aldrich, AA, 1 mM, 72 h); $A\beta_{42}$ oligomers prepared as described in [26] (200 nM, 48 h) in proliferating condition. Control cells were treated with same amount of vehicle (DMSO). Nup153 downregulation was performed by transfecting cells with a mix of three siRNA oligos at 15 nM each (Trilencer-27mer siRNA duplexes, Origene) in Optimem by RNAi max Transfection Agent according to manufacturer's instructions (Thermo Fisher). Nup153 overexpression was performed by Lipofectamine 2000 transfection of a GFP- or a GFP-Nup153 vector (Origene). Each experiment was visually checked for transfection efficiency by analyzing GFP signal. Two days after transfection, neurospheres were dissociated and used either for proliferation assays or for differentiation experiments using Matrigel-coated dishes.

Analysis of NSC Proliferation

Proliferative potential of NSCs was assayed either with 5-bromo-2-deoxy-uridine (BrdU) incorporation or by neurosphere formation assay. Cells were incubated with BrdU (5 μM) for 24 h before fixation in 4% paraformaldehyde for 10 min. After HCl treatment (2 N for 15 min), cells were permeabilized in Triton X-100 (0.3% in PBS) for 15 min and non-specific binding sites were blocked by incubation in 10% BSA for 20 min, and thereafter, primary antibody (rat monoclonal anti-BrdU 1:400, Abcam ab6326) was added for overnight incubation. The following day, after a brief wash, cells were incubated with the TRITC-conjugated secondary antibody (1:500, Invitrogen) for 1 h at room temperature (RT); nuclei were counterstained with DAPI (0.5 mg/mL; Invitrogen) for 10 min.

Neurosphere formation assay was performed using a density of 10 cell/μL to allow the establishment of neurospheres from single cells plated in a 96-plate format. Cells were incubated for 1 week before counting the number of neurospheres. For each independent experiment, the mean number of neurospheres was obtained from eight biological replicates.

Migration Assay

AD-NSCs were transfected with a GFP or a GFP-Nup153 vector as neurospheres and 2 days after dissociated and plated on Matrigel-coated dishes. WT-NSCs were also used as a control. The following day, the monolayer was scraped with a p10 pipe tip in a straight line to create a "scratch." Cell migration was monitored during a time course of 0, 20, and 30 h and images were collected by using a phase-contrast microscope (AXIO microscope equipped with AxioCam ERc5s, Zeiss-objective × 10). Migration was evaluated by measuring the remaining distance between edges in multiple points along the scratch by ZEN imaging software (Zeiss). Data are represented as mean percentage of remaining gap.

Table 1 Primers for gene expression and promoter analyses

TaqMan probes for RT-qPCR target	ID
CYCD1	Mm00432359_m1
GAPDH	Mm99999915_g1
Mash1	Mm03058063_m1
Nup153	Mm00723665_m1
NeuroD1	Mm01280117_m1
Rest	Mm00803268_m1
Tlx (Nr2e1)	Mm00455855_m1
Tbp	Mm01277042_m1
ChIP primers	Sequence
CYCD1 Region 1	F 5′-GAGCGATTTGCATATCTACGAAGGC-3′
CYCD1 Region 1	R 5′-CTCTGGAGGCTGCAGGACTTTGC-3′
CYCD1 Region 2	F 5′-GCTTAACAACAGTAACGTCACACGG-3′
CYCD1 Region 2	R 5′-ATGGTCTCCACTTCGCAGCACAGG-3′

Western Blot, Immunoprecipitation and Antibodies

Protein extracts were prepared in buffer containing 50 mM Tris-HCl (pH 7.4), 250 mM NaCl, 0.1% Triton X-100, 5 mM EDTA, 0.3% Empigen BB, and supplemented with 1 mM PMSF and protease inhibitor mix. Western blot was carried out according to standard procedures and ECL signals were acquired and analyzed with Uvitec imaging system. Optical density values of specific proteins were normalized to that of tubulin, beta-actin, or GAPDH which in our experimental settings were unchanged. Results are expressed as fold change vs wild-type/control samples, which were considered equal to 1. Representative WBs are shown in the figures and graphs show the mean of at least three independent experiments ± standard error of the mean (SEM). The following antibodies were used: anti-Nup153 (WB 1:500; IF 1:400, monoclonal Abcam, ab24700), anti-Nup153 (IP 1:30, monoclonal Abcam, ab93310), anti-Sox2 (WB 1:1000, IF 1:200; polyclonal Abcam, ab97959), anti-DCX (IF 1:200, polyclonal Cell Signalling, 4604), anti-βIII tubulin (WB 1:1000, IF 1:300, polyclonal Abcam, ab18207), anti-MAP2 (IF 1:300, monoclonal Sigma, M9942), anti-GFAP (IF 1:300, polyclonal Cell Signalling, 12389), anti-nitro-tyrosine (WB 1:1000, polyclonal Abcam, ab42789), anti-$Ca_v1.2$ (IF 1:200, polyclonal Millipore, AB5156), anti-H3S10P (IF 1:200, monoclonal, Abcam, ab14955), anti-H3K9-14ac (IF 1:200, polyclonal Cell Signalling, 9677), anti-GAPDH (WB 1:2000, monoclonal Abcam, ab8245), anti-GFP (WB 1:1000, polyclonal Santa Cruz, sc-8334), anti-tubulin (WB 1:4000, monoclonal Abcam, ab7291), anti-beta-actin (WB 1:2000, polyclonal Abcam, ab8227). Aβ oligomers were evaluated by running protein samples onto 10–20% Novex Tricine precast gels (Invitrogen) and probing the membrane with the anti-β-amyloid (WB 1:1000, monoclonal BioLegend, 803014-6E10). In dot blot experiments, 5 μL (15 μg of proteins) of lysate was spotted directly on the membrane. After blocking (milk 5% in TBST), membranes were probed with the anti-β-amyloid or anti-nitro-tyrosine o.n. and then the signal revealed by secondary antibody and ECL reaction as in Western blot. Optical density values of anti-β-amyloid or anti-nitro-tyrosine signals were normalized to red Ponceau staining as indicator of total protein loading. Results are expressed as fold change vs wild-type/control samples, which were considered equal to 1. Co-immunoprecipitation experiments were performed using 3 μg of antibody for 400 μg of protein extract. Ademtech's *Bio-Adembeads* paramagnetic bead system was used to immunoprecipitate the specific proteins. A negative control was performed with the same amount of protein extract sample immunoprecipitated with the corresponding purified IgG (Santa Cruz) (WB: Western blot; IF: immunofluorescence; IP: immunoprecipitation).

Confocal Analysis

Confocal analysis was performed as previously described [9, 27–29]. Cells were fixed in paraformaldehyde for 10 min and then permeabilized for 10 min in 0.2% Triton X-100 in PBS. Mice were anesthetized with a cocktail of ketamine (100 mg/mL) and xylazine (1 mg/mL) and transcardially perfused with saline solution followed by 4% paraformaldehyde. Brains were removed, post-fixed overnight at 4 °C, transferred in a solution of 30% sucrose for 2 days, and then frozen in OCT. Coronal brain sections were cut with a cryostat (40-μm-thick) and processed for immunofluorescence. Free-floating sections were subjected to antigen retrieval in citrate/EDTA buffer pH 6.2 at 95 °C for 5 min and then permeabilized and blocked for 45 min at RT in BSA 5%, NGS 3%, and 0.5% Triton X-100 (Sigma-Aldrich) in PBS. Sections or cells were incubated overnight in primary antibodies as described in the previous paragraph.

The following day, sections or cells were washed in PBS and secondary antibodies added for 1 h. After a brief rinse, nuclei were counterstained with DAPI and slides mounted

with prolong gold antifade. Samples were analyzed with a confocal laser scanning system (Nikon-Ti Eclipse equipped with a × 20-× 40-× 60 objective). Confocal settings were the same for all examined samples to compare fluorescence intensities. 3D images of cells, deriving from reconstruction of z series, were used to calculate the mean fluorescence intensity (MFI) by ImageJ software. Signals from single ROIs were used to calculate the average values for fluorescence intensity; three sections for each animal were analyzed. Nikon-Ti Eclipse software was used to calculate Mander's coefficient for Nup153/Sox2 overlapping in neurospheres and for neurite length measurement in MAP2-positive neurons at D10. Data are presented as mean values ± SEM.

Chromatin Immunoprecipitation

Chromatin immunoprecipitation (ChIP) assays were performed as previously described [30]. Cell lysates were resuspended in 200 μL lysis buffer containing 1% SDS, 50 mM Tris-HCl pH 8.0, and 10 mM EDTA and sonicated on ice with six 10-s pulses with a 20-s interpulse interval. Sample debris was removed by centrifugation and supernatants were precleared with protein G-Sepharose 4B beads (Sigma-Aldrich) for 1 h at 4 °C. Two micrograms of specific antibody or control IgG was added overnight at 4 °C. Immune complexes were collected by incubation with protein G-Sepharose 4B beads for 2 h at 4 °C. After seven washes, immunoprecipitated complexes were separated from beads by vortexing in 150 μL of elution buffer (1% SDS and $NaHCO_3$ 0.1 M; pH 8.0). After addition of NaCl, lysates were incubated overnight at 65 °C to reverse protein-DNA cross-linking. Chromatin fragments were extracted with PCR DNA fragments purification kit (Geneaid). PCR conditions and cycle numbers were determined empirically, and each PCR reaction was performed in triplicate. Data are expressed as percentage of input calculated by the "adjusted input value" method according to the manufacturer's instructions (Thermo Fisher scientific ChIP analysis). To calculate the adjusted input, the Ct value of input was subtracted by 6.644 (i.e., log2 of 100). Next, the percent input of control and IP samples was calculated using the formula: 100 × 2 (adjusted input − Ct(ChIP)). The percent input of IgG samples was calculated using the formula 100 × 2 (adjusted input − Ct(IgG)). Primers used for promoter analysis are indicated in Table 1.

Electrophysiology

Voltage-clamp recordings of Na^+ currents were performed at RT by means of a Multiclamp 700B/Digidata 1550A system (Molecular Devices, USA) in NSCs induced to differentiate for 14 days. Membrane capacitance and series resistance were estimated by the dial settings on the amplifier. Capacitive transients and series resistance were compensated electronically by 75–85% [31]. Cells with series resistance more than 25 mΩ were not considered for analysis. Current signals were low-pass filtered and digitized at 10 kHz sampling frequency. Patch electrodes, fabricated from borosilicate glass capillaries with the aid of a micropipette puller (P-97; Sutter Instruments), had resistances of 3–5 MΩ when filled with the internal solution that contained the following (in mM): 120 CsCl, 10 NaCl; 20 TEA-Cl; 10 EGTA, 10 Hepes; 2 MgCl2, 4 NaATP, (pH 7.4 with CsOH). For recordings, cells were perfused with an external Tyrode solution containing the following (in mM): 135 NaCl, 1 $CaCl_2$, 2 $MgSO_4$, 10 HEPES, 10 glucose, 5 TEA-Cl, and 0.2 CdCl (pH 7.4). Voltage-dependent inward currents were evoked by 125 ms depolarizing pulses with 10 s interpulse interval to test potentials between − 80 and + 40 mV (10 mV increments) from a holding potential of − 90 mV. Currents were on-line leak subtracted via a P/4 routine. Current density was obtained by dividing Na^+ current amplitude by membrane capacitance. Membrane capacitance was calculated by dividing the integral of the uncompensated capacitive current produced by a voltage step of − 10 mV (the capacitive charge movement) by the amplitude of the voltage step itself [32].

Statistics

Data are expressed as mean of independent experiments ± SEM calculated with Sigmaplot software. Sample size (n) is indicated in the figure legend and represents independent experiments from different cell culture preparations or animals. Significance in normally distributed samples was analyzed using a two-tailed Student's t test and one-way analysis of variance (ANOVA) followed by post hoc tests (Student-Newman-Keules (SNK), Bonferroni, Holm-Šídák) for multiple comparisons. In the other cases, non-parametric tests (Mann-Whitney U test or ANOVA on RANKS followed by post hoc tests), as indicated in the figure legends, were applied. p values < 0.05 were considered as significant in all tests. For all analyses, the observer was blind to the identity of the samples.

Results

Nup153 Expression Is Reduced in Hippocampal NSCs from 3×Tg-AD Mice

Since defects in proliferation and maturation processes have been described in NSCs isolated from the 3×Tg-AD mouse model (AD-NSCs) [33], we hypothesized that expression and/or function of Nup153, which acts as a modulator of both processes [12], could be altered in these cells. To address this issue, we performed ex vivo confocal microscopy analysis of Nup153 expression within the hippocampal niche of young

(2-month-old) 3×Tg-AD mice and age-matched WT control mice. As expected Nup153 was well expressed in NSCs, specifically located in the hippocampal subgranular zone of WT mice, also positive for the neural stem/progenitor cell marker Sox2 (Fig. 1a). Interestingly, Nup153 expression was reduced in all the cells of the hippocampal DG of young 3×Tg-AD mice, including those positive for Sox2 (mean fluorescent intensity (MFI) 132.77 ± 2.75 WT vs 45.69 ± 4.28 AD, Student's t test, $p < 0.001$; Fig. 1b). Indeed, a reduction of 40% in Nup153 level was found by WB analysis in total

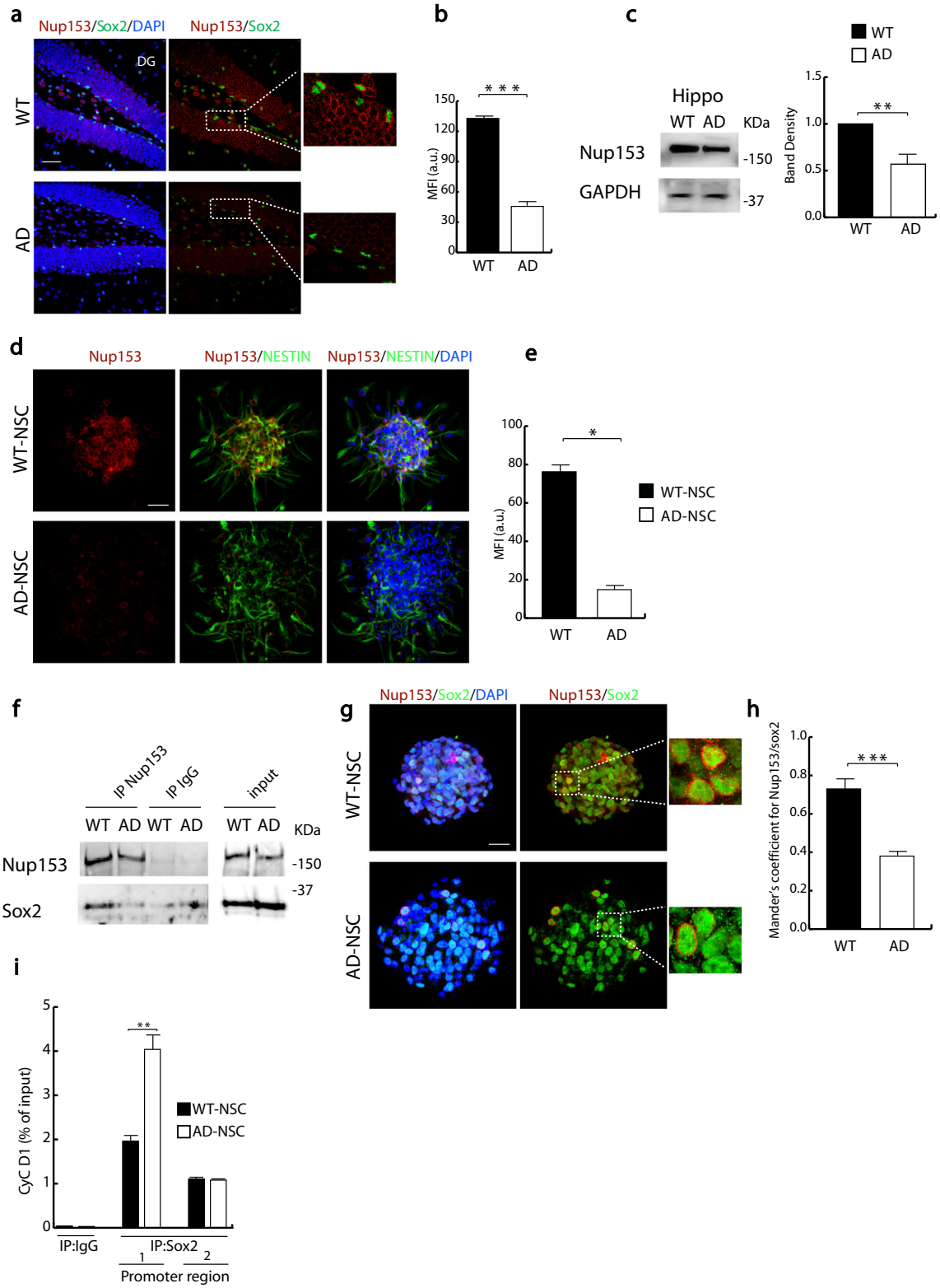

◀ **Fig. 1** AD-NSCs exhibit low Nup153 levels and decreased association with Sox2. Confocal analysis of Nup153 and Sox2 expression in the DG from 2-month-old WT and AD mice (**a**). Right panels show enlargements. Nuclei were counterstained with DAPI, scale bar 50 μm. **b** Mean fluorescence intensity (MFI) analysis relative to Nup153 level in $Sox2^+$ NSCs in WT and AD mice (Student's *t* test, $n = 4$). **c** Western blot showing Nup153 levels in hippocampal extracts from 2-month-old WT and AD mice. The graph shows the densitometric analysis (Student's *t* test, $n = 4$). **d** Confocal analysis of Nup153 expression in nestin-positive neurospheres isolated from WT and AD newborn mice, scale bar 50 μm. **e** Mean fluorescence intensity (MFI) analysis relative to Nup153 level in neurospheres (Mann-Whitney *U* test, $n = 4$). **f** Co-IP showing the association of Nup153 with Sox2 in extracts from WT and AD-NSCs ($n = 3$). **g** Confocal analysis of neurospheres derived from WT and AD mice co-labeled with Nup153 and Sox2 (scale bar 50 μm). Nuclei were counterstained with DAPI. Higher magnification images are shown in the insets. **h** Mander's coefficient relative to Nup153/Sox2 association in WT and AD neurospheres (Student's *t* test, $n = 4$). **i** Chromatin immunoprecipitation showing Sox2 binding to CycD1 promoter (two different regions are shown) expressed as % of input in WT- and AD-NSCs (Student's *t* test, $n = 3$). Data plotted as mean ± SEM, $*p < 0.05$, $**p < 0.01$, $***p < 0.001$

hippocampal extracts of 3×Tg-AD mice (Fig. 1c) compared to age-matched WT mice (Student's *t* test, $p < 0.01$).

Compelling evidence indicates that NSCs residing in the granular cell layer of the adult hippocampal DG are morphologically distinguishable in radial and non-radial cells. Although both cell types co-express Sox2 and brain lipid-binding protein (BLBP), the radial cells are commonly quiescent while the non-radial cells are activated and they respond differently to neurogenic stimuli [34]. For this reason, we wondered whether they could be characterized by different Nup153 expression levels. Confocal analysis of GFAP-positive NSCs showing radial or horizontal morphology in the DG revealed that Nup153 levels were similar in the two subpopulations of both WT and AD mice. In line with other results, the levels of Nup153 were consistently lower in both radial and non-radial NSCs from AD mice compared to those measured in WT mice (MFI: 167.39 ± 14.20 WT-radial, 165.33 ± 13.96 WT-non-radial; 38.65 ± 4.82 AD-radial, 37.42 ± 4.51 AD-non-radial; ANOVA, Bonferroni test, $p < 0.001$; Supplementary Fig. 1a, b, c).

A significant Nup153 reduction was evident also in AD-NSCs, cultured in vitro as neurospheres and co-labeled with the stemness marker nestin, compared to WT-NSCs (Fig. 1d, e). Specifically, the MFI, expressed in arbitrary units, was 76.23 ± 3.56 in WT-NSCs and 14.82 ± 1.15 in AD-NSCs (Mann-Whitney *U* test, $p < 0.05$).

Several works, including ours [9], have reported that Nups may control and interact with chromatin remodeling enzymes [8] and transcriptional factors providing an epigenetic platform helping to dynamically regulate gene expression [8]. Along this line, very recently, the association of Nup153 with the transcription factor Sox2 has been described to be crucial for NSC maintenance and fate determination [12]. Thus, we asked whether reduced Nup153 levels in AD-NSCs also altered the formation of this important complex. Co-IP experiments revealed that the Nup153/Sox2 complex was strongly reduced in AD-NSCs compared to WT-NSCs (Fig. 1f). Accordingly, confocal analysis showed that Nup153 and Sox2 co-localization in AD-NSC neurospheres was reduced compared to those deriving from WT-NSCs (Mander's coefficient for Sox2/Nup153 association WT 0.73 ± 0.05 vs AD 0.38 ± 0.02, Student's *t* test, $p < 0.001$; Fig. 1g, h). Since a deregulation of Sox2 function and genomic localization has been found after Nup153 silencing in neural progenitors [12], we hypothesized that reduction in Nup153 levels and complex formation with Sox2 that we found in AD-NSCs could alter the Sox2-dependent gene regulation in these cells. By chromatin immunoprecipitation, we investigated Sox2 recruitment on two different regions of the CycD1 promoter. Fine-tuned repression of CycD1 by Sox2 is necessary for the maintenance of slow-dividing multipotent neural progenitors [35]. We found that Sox2 recruitment on CycD1 promoter region 1 was higher in AD-NSCs compared to WT-NSCs suggesting a stronger repression of this gene in AD-NSCs (WT-NSCs 1.96 ± 0.08 vs AD-NSCs 4.04 ± 0.39, Student's *t* test, $p < 0.01$; Fig. 1i). The binding of Sox2 in the second region analyzed was similar in WT- and AD-NSCs.

Altered Nitric Oxide Signaling and Aβ Accumulation Affect Nup153 Levels in AD-NSCs

Next, we asked whether ˙NO signaling is involved in Nup153 downregulation observed in our AD-NSC model. To address this issue, we first exposed proliferating WT-NSCs to the ˙NO donor DETANO (100 μM for 24 h) or to the pan-NOS inhibitor LNAME (5 mM for 72 h). WB analysis revealed that Nup153 was downregulated or upregulated in the presence of DETANO and LNAME, respectively (DETANO 0.64 ± 0.06, LN 1.80 ± 0.12, fold change vs Control, ANOVA on RANKS, SNK test, $p < 0.05$; Fig. 2a). Since Aβ accumulation has been linked to the generation of oxidative/nitrosative stress also in stem cells from APP23 AD mouse [18], we investigated the contribution of Aβ to Nup153 levels in NSCs. First, by dot blot experiments, we confirmed Aβ accumulation in AD-NSCs deriving from 3×Tg-AD mice that was significantly reduced by 72-h treatment with a γ-secretase inhibitor (GSI, 1 μM) (AD-NSCs 5.29 ± 0.79, AD-NSCs-GSI 1.54 ± 0.37 fold change vs WT-NSCs, ANOVA, Bonferroni test, $p < 0.001$; Supplementary Fig. 2a). We also analyzed the Aβ oligomer distribution pattern in AD-NSCs and we found several oligomers, including trimers and tetramers in AD-NSCs similarly to what observed in hippocampal tissue lysates from 9-month-old 3×Tg-AD mice that we used as positive control. Hippocampal tissue lysates from APP knock-out mice lacking Aβ oligomers were used as negative control (Supplementary Fig. 2b).

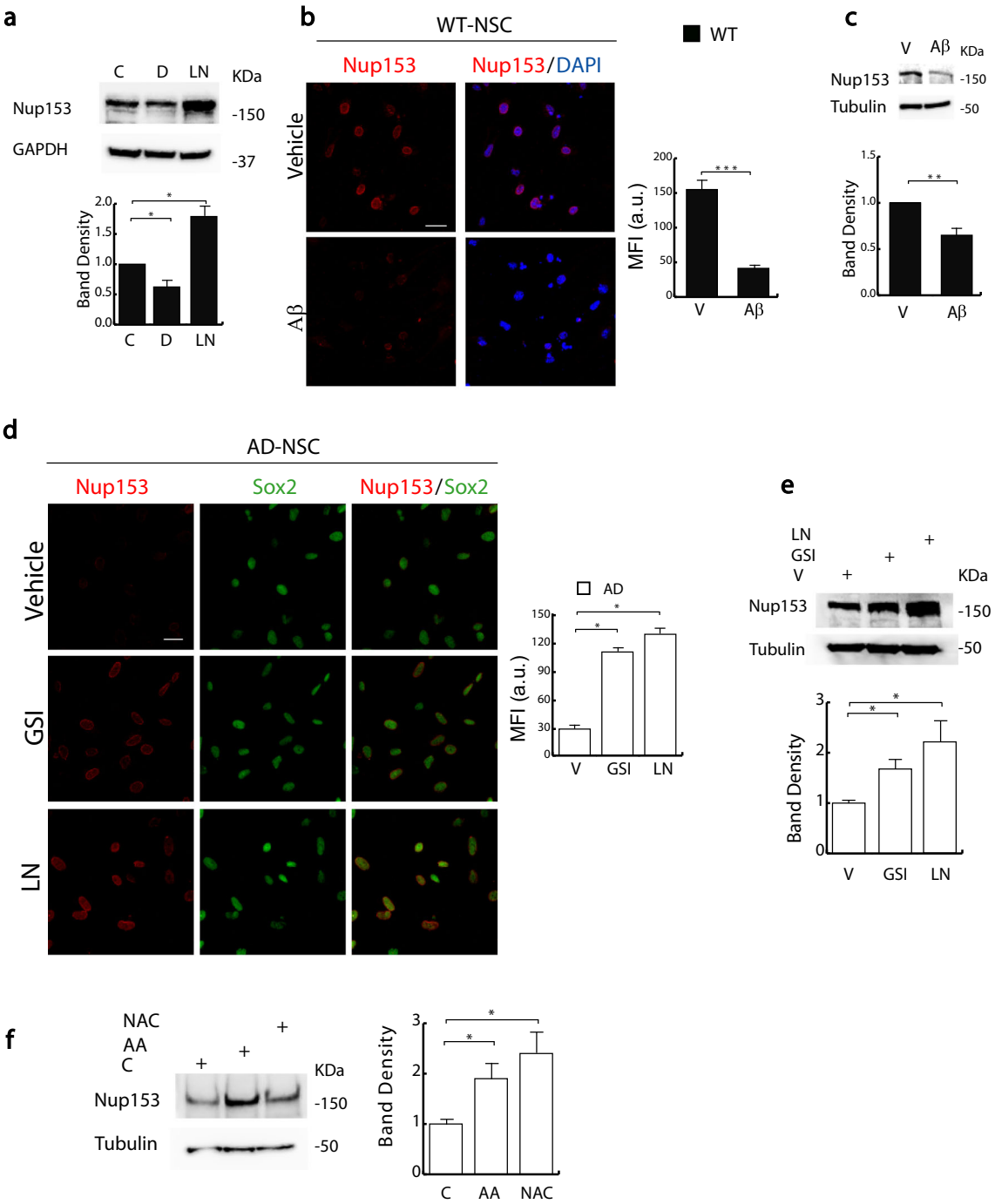

Fig. 2 Nitrosative stress and Aβ regulate Nup153 levels in AD-NSCs. **a** Nup153 protein levels assessed by WB analysis in WT-NSCs treated with DETANO (D, 100 μM, 24 h) or LNAME (LN, 5 mM, 3 days). The bar graph shows the densitometric analysis (ANOVA on RANKS, SKN test, $n = 5$). **b** Confocal analysis of Nup153 expression in WT-NSCs treated with vehicle (V) or Aβ (200 nM) for 48 h. Nuclei were counterstained with DAPI, scale bar 50 μm. Mean fluorescence intensity (MFI) analysis relative to Nup153 level is shown in the right panel (Student's *t* test, a.u. arbitrary units, $n = 4$). **c** WB analysis of Nup153 expression in WT-NSCs in proliferating condition and treated with either vehicle or Aβ (200 nM) for 48 h. Bar graph shows the densitometric analysis (Student's *t* test, $n = 3$). **d**, **e** Expression of Nup153 and Sox2 in AD-NSCs treated with either LNAME (5 mM) or γ-secretase inhibitor (GSI, 1 μM) for 72 h, compared to vehicle-treated cells analyzed by confocal microscopy (**d**) or by WB (**e**). Scale bar 20 μm. WB quantification: ANOVA on RANKS, SKN test ($n = 4$); MFI analysis relative to Nup153 level is also shown (ANOVA on RANKS, SKN test, $n = 4$, a.u. arbitrary units). **f** WB analysis of Nup153 levels in AD-NSCs treated with either ascorbic acid (AA, 1 mM) or *N*-acetylcysteine (NAC, 5 mM) for 72 h (ANOVA on RANKS, SKN test, $n = 4$). Data plotted as mean ± SEM, $^{*}p < 0.05$, $^{**}p < 0.01$, $^{***}p < 0.001$

To address whether Aβ accumulation affected Nup153 expression, we exposed WT-NSCs to 200 nM Aβ for 48 h. In this condition, we found decreased levels of Nup153, as assessed by semi-quantitative MFI analysis of confocal

images (WT-NSC-vehicle 155.60 ± 21.37 vs WT-NSCS-Aβ 41.34 ± 2.12, Student's *t* test, $p < 0.01$; Fig. 2b) and WB (Aβ 0.62 ± 0.05, fold change vs vehicle, Student's *t* test, $p < 0.01$; Fig. 2c). To further address the contribution of Aβ and nitrosative stress to Nup153 levels in AD-NSCs, we treated these cells for 72 h with the γ-secretase inhibitor (GSI, 1 μM), to reduce the cleavage of β-amyloid precursor protein and the generation of its toxic peptide, or with the pan-NOS inhibitor LNAME (5 mM for 72 h), which not only decreases ˙NO levels but is efficient in reducing nitro-tyrosine protein levels in AD-NSCs, as shown in the dot blot assay (LN 0.46 ± 0.014 fold decrease vs vehicle, Student's *t* test, $p < 0.001$, Supplementary Fig. 3a, b). A recovery of Nup153 protein level was observed, in the above conditions, by WB, confocal analyses, and the relative MFI (MFI: vehicle 28.76 ± 1.50, GSI 114.85 ± 7.70, LN 128.36 ± 11.50 ANOVA on RANKS, SNK test, $p < 0.05$; Fig. 2d); (WB: GSI 1.67 ± 0.04, LN 2.20 ± 0.66 fold change vs control, ANOVA on RANKS, SNK test, $p < 0.05$; Fig. 2e). Moreover, 72-h treatment of AD-NSCs with either the antioxidant compounds *N*-acetylcysteine (NAC, 5 mM) or ascorbic acid (AA, 1 mM) increased the level of Nup153 (AA 1.97 ± 0.29, NAC 2.46 ± 0.49 fold change vs vehicle, ANOVA on RANKS, SNK test, $p < 0.05$; Fig. 2f). These data point to a cross-talk between Aβ and oxidative/nitrosative stress in Nup153 downregulation observed in our AD-NSC model.

Nup153 Restoration in AD-NSCs Promotes Their Proliferation

As previously reported, Nup153 is crucial for the maintenance of NSC properties, including proliferation [12]. To further address this point, we silenced or overexpressed Nup153 protein in WT-neurospheres either by siRNA or by means of a GFP-Nup153 plasmid and compared them to those transfected with scramble oligos or a GFP-empty vector respectively as showed in Supplementary Fig. 4a. Nup153 silencing in WT-NSCs reduced the number of neurospheres, whereas Nup153 overexpression increased it compared to control cells (siRNA 0.48 ± 0.05 fold change vs scramble, GFP-Nup 1.93 ± 0.03 vs GFP, ANOVA, Bonferroni test, $p < 0.001$; Supplementary Fig. 4b). To understand whether Nup153 overexpression might regulate proliferation also in AD-NSCs, we transfected these cells with a Nup153 GFP-tagged vector or a GFP-control vector. Transfection efficiency was checked by confocal analysis of GFP signal (% of GFP^+ cells: 69.79 ± 0.74 GFP vs 60.1 ± 2.02 Nup-GFP; Supplementary Fig. 5a, b). Furthermore, as shown in Fig. 3a, b, Nup153 protein and mRNA levels were efficiently increased in AD-NSCs overexpressing Nup153 as compared to GFP-transfected cells and WT-NSCs (WB: WT-NSCs 4.76 ± 1.76, AD-NSC-Nup 1.86 ± 0.32 fold change vs AD-NSCS-GFP, ANOVA on Ranks, SNK test, $p < 0.05$) (RNA: AD-NSCs 0.62 ± 0.03, AD-NSC-Nup 197.07 ± 21.77 fold change vs WT, ANOVA on RANKS, Holm-Šídák test, $p < 0.01$). In these conditions, we analyzed the phosphorylation level of serine 10 on histone H3 (H3S10p) that is an epigenetic mark associated with cell proliferation. H3S10p levels, low in AD-NSCs in comparison to WT-NSCs, were partially restored by Nup153 overexpression, as shown by confocal analysis and MFI analysis (WT-NSCs 351.58 ± 28.35, AD-NSC-GFP 86.24 ± 14.52, AD-NSC-Nup 189.73 ± 13.71, ANOVA, Bonferroni test, $p < 0.05$; Fig. 3c). Similar results were obtained on acetylation levels of lysines 9 and 14 on H3 (H3K9-14ac), associated with chromatin activation, that were increased in Nup153-overexpressing AD neurospheres compared to AD-GFP-neurospheres (Supplementary Fig. 6). Proliferation analysis by BrdU incorporation test also revealed that Nup153 overexpression significantly increased AD-NSC proliferation. As control, we also overexpressed or silenced Nup153 in WT-NSCs and found that it increased or decreased BrdU incorporation respectively (Fig. 3d) compared to GFP- or scramble-transfected control cells. Specifically, the percentages of BrdU-positive cells were as follows: WT-NSC-sc 57.55 ± 3.33, WT-NSC-siNup 32.75 ± 2.65, WT-GFP 54.0 ± 2.96, WT-Nup 91.82 ± 4.24, AD-NSC-GFP 33.84 ± 1.07, AD-NSC-Nup 69.05 ± 4.57, ANOVA, SNK test, $p < 0.01$). In addition, the number of neurospheres, as well as their size, was increased in AD-NSCs overexpressing Nup153 (no. of neurospheres: AD-NSC-Nup 1.90 ± 0.04 fold change vs AD-NSC-GFP, ANOVA, Bonferroni, $p < 0.05$) (area: AD-NSC-Nup 14,265.98 ± 1743.89, AD-NSC-GFP 6611.32 ± 1292.70, Student's *t* test, $p < 0.05$; Fig. 3e, f). In parallel, we analyzed by RT-qPCR the expression level of CycD1 and TLX/NR2E1, two genes mainly involved in regulation of NSC proliferation and self-renewal capacity. Interestingly, both CycD1 and TLX/NR2E1 mRNA were significantly downregulated in AD-NSCs compared to WT-NSCs, but their relative expression was completely restored in Nup153-transfected AD-NSCs (CycD1: WT-NSCs 1.00 ± 0.07, AD-NSC-GFP 0.78 ± 0.01, AD-NSC-Nup 1.16 ± 0.03; TLX: WT-NSCs 1.00 ± 0.03, AD-NSC-GFP 0.70 ± 0.01, AD-NSC-Nup 1.19 ± 0.07, ANOVA on RANKS, Holm-Šídák, $p < 0.001$; Fig. 3g).

Nup153 Restoration in AD-NSCs Promotes Their Migration

Further experiments were designed to address whether Nup153 restoration could also ameliorate NSC migration, an event important for next terminal neuronal differentiation and functional integration. The ability of GFP- or Nup153-transfected AD-NSCs to close the scratch over time was evaluated and compared to WT-NSCs. This test revealed that Nup153 upregulation in AD-NSCs recovered their ability to migrate in a manner similar to WT cells (% remaining gap: WT-NSCs 38.4 ± 3.1, AD-NSC-

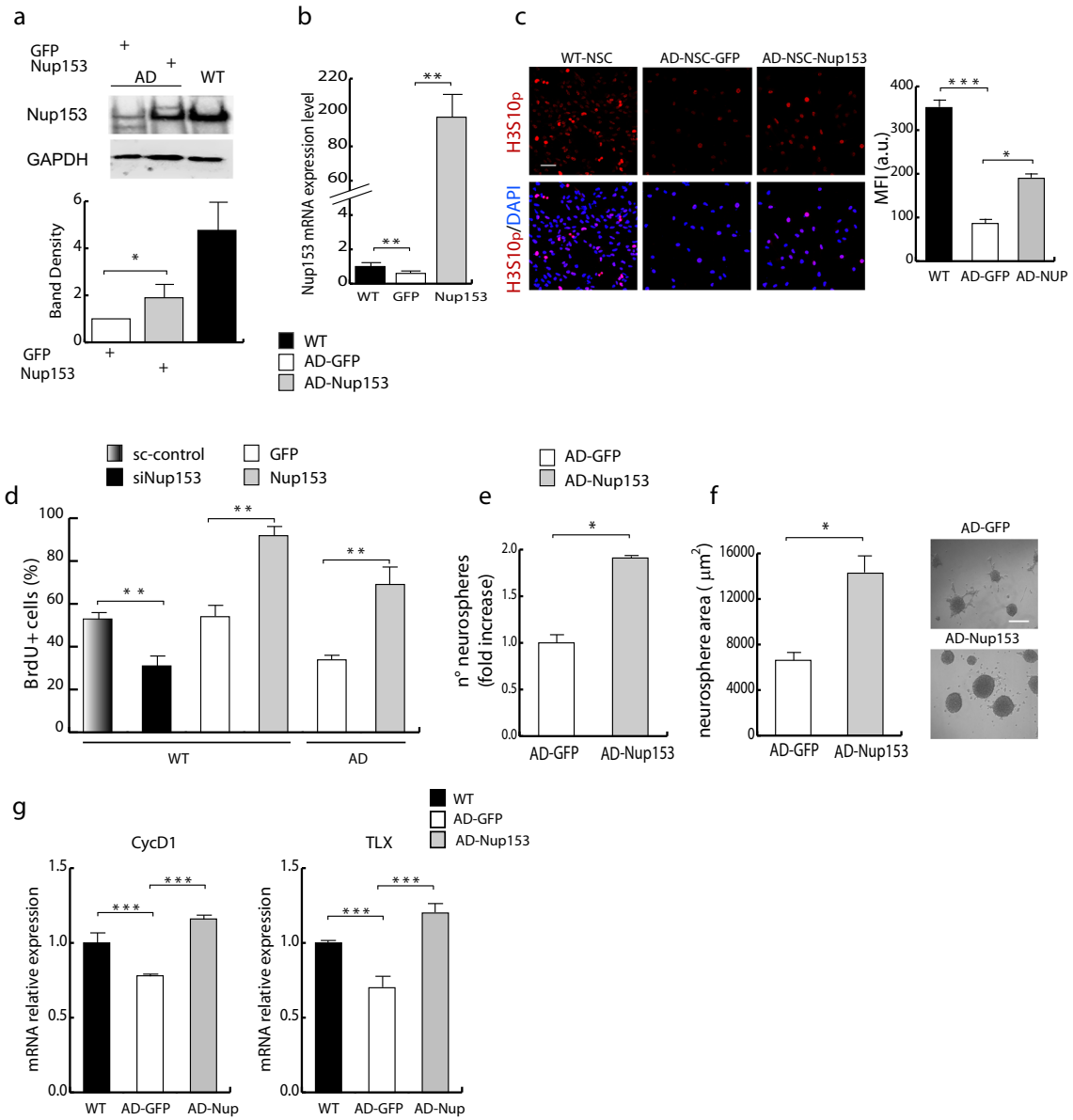

Fig. 3 Nup153 overexpression increases the proliferative capacity of AD-NSCs. **a** Representative WB showing Nup153 levels in WT and in AD-NSCs transfected with a GFP or a GFP-Nup153 vector. The graph shows the densitometric analysis (ANOVA on RANKS, SKN test, $n = 3$). **b** Bar graph representing RT-qPCR analysis for Nup153 mRNA levels in WT-NSCs and AD-NSCs, overexpressing GFP or Nup153 vectors, respectively (ANOVA on RANKS, Holm-Šídák test, $n = 3$). **c** Representative images of H3S10p levels in WT or AD-NSCs expressing a GFP or a GFP-Nup153 vectors. Nuclei were counterstained with DAPI (scale bar 50 µm). Mean fluorescence intensity (MFI) analysis relative to H3S10p level is shown in the right panel (ANOVA, Bonferroni test, $n = 4$, a.u arbitrary units). **d** Percentage of BrdU incorporation in scramble- or siNup153-treated WT-NSCs or in AD-NSCs overexpressing a Nup153 or a control vector (ANOVA, SKN test, $n = 4$). **e** Neurosphere assay in AD-NSCs transfected with GFP- or GFP-Nup153 vectors (Student's t test, $n = 3$). **f** Neurosphere area calculated from experiments in **e** (Student's t test, $n = 4$) with representative images shown on the right (scale bar 100 µm). **g** CycD1 and Tlx mRNA expression by RT-qPCR in WT- and AD-NSCs expressing GFP or a GFP-Nup153 vector (ANOVA on RANKS, Holm-Šídák test, $n = 3$). Data plotted as mean ± SEM, $^{*}p < 0.05$, $^{**}p < 0.01$, $^{***}p < 0.001$

GFP 58.7 ± 3.8, AD-NSC-Nup 31.8 ± 2.2, ANOVA, Bonferroni test, $p < 0.001$; Fig. 4a). The polysialylated form of NCAM plays an important role in neural cell migration and invasion [36] reducing cell adhesion. Of note, its expression is strongly reduced in glial progenitor cells isolated from cortical tissue of AD patients or APP23 AD-model [18]. Confocal analysis showed that PSA-NCAM level, reduced in AD-NSCs compared to WT-NSCs, was increased in AD-NSCs transfected with the vector for Nup153 suggesting that Nup153 may, at least in part, regulate migration through PSA-NCAM modulation (MFI: WT-NSCs 558.9 ± 80.7, AD-NSC-GFP 77.5 ± 15.5, AD-NSC-Nup 277.2 ± 60.8, ANOVA, SNK test, $p < 0.05$; Fig. 4b).

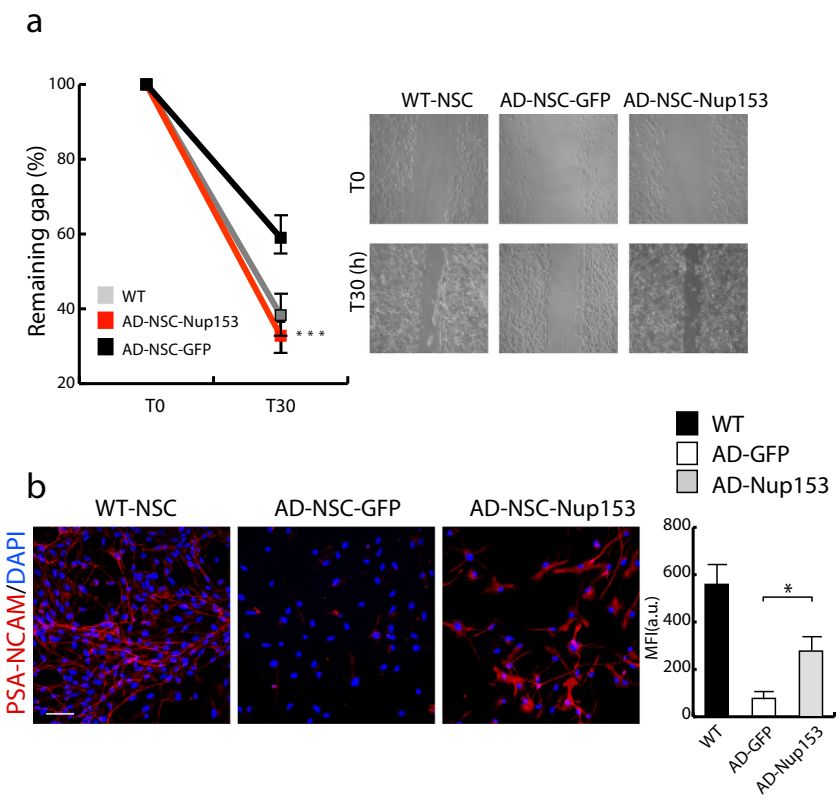

Fig. 4 Nup153 overexpression increases migration of AD-NSCs. **a** Migration assay in AD-NSCs overexpressing a GFP or a GFP-Nup153 vector compared to WT-NSCs ($p < 0.001$ vs GFP, ANOVA, Bonferroni test, $n = 4$). Representative images of scratch assay are shown in the right panels, scale bar 100 μm. **b** Confocal analysis of PSA-NCAM expression in the above conditions. Scale bar 50 μm. Nuclei were counterstained with DAPI. The bar graph shows the MFI analysis of PSA-NCAM fluorescence signal in WT- and AD-NSCs expressing GFP or GFP-Nup153 vectors (ANOVA, SNK test). Data plotted as mean ± SEM, $p < 0.05$, $^{***}p < 0.001$

Nup153 Overexpression Recovers AD-NSC Response to Differentiation

Next, we investigated the role of Nup153 in AD-NSC differentiation. It has been reported that Nup153 silencing may produce different effects on neurogenesis depending on the context in which it operates [12]. We therefore asked whether this important epigenetic factor plays similar or different roles in neuronal differentiation of AD- and WT-NSCs.

To address this issue, we started characterizing the role of Nup153 in our experimental model of WT-NSCs. Confocal analyses showed that Nup153, highly expressed in proliferating undifferentiated WT-NSCs, was downregulated during differentiation along with the acquisition of the early differentiation marker DCX (Supplementary Fig. 7a). More interestingly, we found that Nup153 silencing in WT-NSCs induced an early expression of the determination genes Mef2c, Mash1, and NeuroD1, as revealed by RT-qPCR analysis (Supplementary Fig. 7b) at 48 h (D2) (Mef2c 1.70 ± 0.18; Mash1 1.87 ± 0.07; NeuroD1 1.90 ± 0.05 fold change siNup vs scramble, Student's *t* test, $p < 0.05$). Confocal analysis also revealed that β-III tubulin- and MAP2-positive neurons, deriving from Nup153-silenced WT-NSCs and analyzed at D6, showed a more complex arborization and branching (neurite length (μm): scramble 128.5 ± 4.2, siNup 194.9 ± 8.4 ANOVA, Bonferroni test, $p < 0.01$; Supplementary Fig. 7c, d). Accordingly, electrophysiological recordings performed in scramble- or Nup153 silenced-WT-NSCs (siNup153), induced to differentiate for 14 days, revealed that Na^+ current density was significantly increased (Supplementary Fig. 7e) in cells depleted of Nup153, suggesting an earlier maturation of these cells.

Collectively, data reported above indicate that Nup153 overexpression increases the proliferative capacity of WT-NSCs whereas, under differentiative conditions, Nup153 downregulation promotes a better differentiation.

We then moved to our AD model of NSCs and investigated the expression of the early determination genes Mash1, NeuroD1, and REST in differentiating AD-NSCs previously transfected with GFP or Nup153-vectors. RT-qPCR analysis revealed that in Nup153-overexpressing AD-NSCs, Mash1, NeuroD1, and REST expression was significantly higher compared with GFP-overexpressing AD-NSCs (Mash1 1.31 ± 0.15, NeuroD1 1.62 ± 0.21, REST 1.53 ± 0.26 fold change vs AD-NSC-GFP, ANOVA on RANKS, Holm-Šídák test, $p < 0.05$ and $p < 0.001$; Fig. 5a), and it was paralleled by a higher number of DCX^+ cells at D3, as evaluated by confocal analysis (% DCX^+ cells, AD-NSC-GFP 5.36 ± 0.60, AD-NSC-Nup 12.56 ± 2.94, Mann-Whitney *U* test, $p < 0.01$; Fig. 5b, c). Western blot analysis revealed that Nup153, upregulated in AD-NSCs after transfection in proliferative conditions, was however downregulated at D3 when DCX expression increased (Fig. 5d). Conversely, GFP level in GFP-transfected AD-NSCs was not significantly diminished after

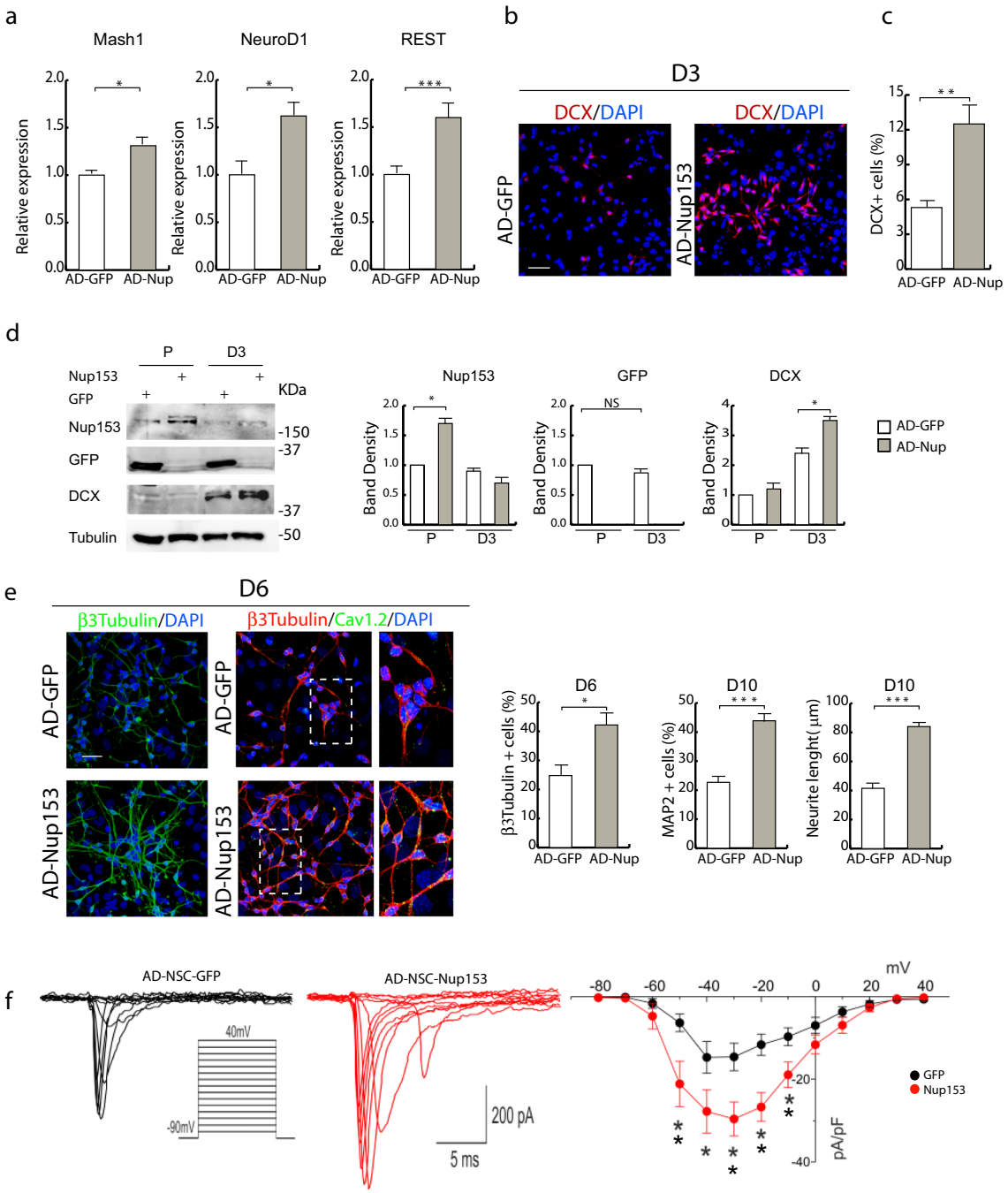

Fig. 5 Nup153 overexpression restores the response of AD-NSCs to differentiation stimulus. **a** Bar graphs showing RT-qPCR analysis for Mash1, NeuroD1, and REST mRNA expression levels in AD-NSCs transfected with GFP or GFP-Nup153 vectors and then induced to differentiate for 1 (Mash1, NeuroD1) or 2 days (REST) (ANOVA on RANKS, Holm-Šídák test, $n = 3$). **b**, **c** Representative images (**b**) and quantification (**c**) of DCX-positive cells (%, Mann-Whitney U test, $n = 5$) in GFP- or GFP-Nup153-transfected AD-NSCs at D3. Nuclei were counterstained with DAPI, scale bar 50 μm. **d** Western blot showing the protein levels of Nup153, GFP, and DCX relative to tubulin, used as loading control, in proliferation condition and at D3 in GFP- and GFP-Nup153-transfected AD-NSCs. Densitometric analysis is provided in the right panels (Nup153: ANOVA, Bonferroni test; GFP: Student's t test; DCX: ANOVA, Holm-Šídák test, $n = 3$). **e** Representative images of β-III tubulin expression in GFP- or GFP-Nup153-transfected AD-NSCs at D6 (left panels). Calcium channel ($Ca_v1.2$) expression is visualized in the same conditions in β-III tubulin$^+$ neurons (right panels). Higher magnification images show $Ca_v1.2$ expression in the cell body and in dendrites of β-III tubulin$^+$ neurons. Nuclei were counterstained with DAPI, scale bar 50 μm. The graphs show the percentage of β-III tubulin$^+$ neurons at D6 (Student's t test, $n = 7$), and the percentage (Student's t test, $n = 7$) and mean neurite length (Student's t test, $n = 5$) of MAP2$^+$ neurons at D10. **f** Representative traces of voltage-gated Na^+ currents evoked by a series of depolarizing steps from −90 to +40 mV in GFP- or Nup153-overexpressing AD-NSCs. Inset: voltage protocols. The right panel shows current-to-voltage relationship of peak Na^+ current densities for NSCs in the above conditions (black circles, GFP; red circles, Nup153) (Student's t test, GFP $n = 15$, Nup $n = 16$). Data plotted as mean ± SEM, $p < 0.05$ $^{**}p < 0.01$, $^{***}p < 0.001$

3 days of differentiation (Fig. 5d). Analysis at D6 of neurons derived from Nup153-transfected AD-NSCs showed increased complexity and arborization compared to control cells (Fig. 5e) along with higher expression of the calcium channel $Ca_v1.2$, as assessed by confocal analysis. The number of neurons positive for β-III tubulin at D6 and MAP2 at D10 was higher in cells that were subjected to Nup153 overexpression (% β-III tubulin$^+$ cells, AD-NSC-GFP 24.84 ± 4.67, AD-NSC-Nup 42.21 ± 4.52, Student's t test, $p < 0.05$; % MAP2$^+$ cells AD-NSC-GFP 22.76 ± 2.09, AD-NSC-Nup 43.89 ± 2.38, Student's t test, $p < 0.001$). Likewise, neurite length, measured at D10, was increased in neurons deriving from AD-NSCs transfected with Nup153 in comparison to those deriving from control AD-NSCs (AD-NSC-GFP 41.56 ± 2.92, AD-NSC-Nup 84.26 ± 2.45 (μm), Student's t test, $p < 0.001$; Fig. 5e). Accordingly, in neurons deriving from Nup153 overexpressing AD-NSCs, we found increased Na^+ current density compared to those deriving from control AD cells (Fig. 5f) indicating a Nup153-dependent functional recovery and increased maturation at D14.

Discussion

Neural stem cell fate is regulated by the interplay of many epigenetic factors. Among these, Nup153 recently emerged as a master regulator of gene expression in several contexts including embryonic and neural progenitor cell fate [11, 12]. Here, we show that alteration of Nup153 expression in NSCs deriving from AD mice reduced their potential and function.

Indeed, Nup153 maintains NSC pluripotency and regulates adult neurogenesis in normal condition [12]. In agreement with these data, we found that Nup153 overexpression in WT-NSCs promoted cell proliferation whereas its downregulation produced the opposite effect. WT-NSCs, transiently silenced for Nup153 and induced to differentiate in vitro, showed an early expression of neuronal markers paralleled by mature and electrically competent phenotype compared to controls. These results indicate that a temporary reduction of Nup153 levels during the early phases of differentiation may facilitate the maturation of NSCs towards a neuronal phenotype.

However, Nup153 silencing has been previously reported [12] to produce different effects on neurogenesis depending on the context (in vivo vs in vitro) and culture conditions. These different outcomes are not surprising considering that Nup153 may act as an epigenetic hub for many co-regulators in order to either activate or repress stemness/lineage-specific genes. In the light of these considerations, Nup153 modulation for therapeutic NSC-based strategies should imply an approach allowing a tight and timely regulation of its expression.

In the pathological context of AD, we found that overexpressing Nup153 in AD-NSCs recovered their proliferative capacity and migration. Surprisingly, Nup153 upregulation in AD-NSCs did not inhibit their differentiation. Actually, when AD-NSCs overexpressing Nup153 were induced to differentiate, we found more neurons that also showed increased dendritic arborization and a more mature electrophysiological competent phenotype. These data suggest that the positive effect of Nup153 restoration in the differentiation of AD-NSCs is not merely based on the increased availability of differentiating cells because of Nup153 positive action on proliferation. Remarkably, Nup153 also actively affects the differentiation process by promoting the expression of proneural genes and favoring the acquisition of a mature neuronal phenotype. Of note, Nup153, efficiently overexpressed after transfection in proliferative conditions, was however downregulated upon differentiation. These results suggest that the mechanisms responsible for the physiological Nup153 decrease occurring during differentiation are still active in AD regardless of transfection. More importantly, these data suggest that the rescue of Nup153 level in proliferating neural precursors restores their plasticity and their proficiency for either proliferative or differentiative stimuli.

As reported previously, Nup153 in association with Sox2 controls NSC function by epigenetic mechanisms [12]. In addition, Sox2 has been reported as a key regulator of cortical progenitors by maintaining the population in a slowly dividing and self-renewing state through a fine-tuned repression of proliferation genes such as CycD1 [35]. Upon differentiation, Sox2 occupancy on CycD1 promoter is decreased allowing the transition of stem cells towards rapidly dividing cells and then towards differentiation-committed cells. In the pathological context of AD however, both the formation of Nup153/Sox2 complex and the function of Sox2 are affected by reduced Nup153 levels. In fact, in AD-NSCs Sox2 recruitment on CycD1 promoter is increased compared to WT-NSCs and paralleled by lower CycD1 gene expression. Of note, Nup153 overexpression recovers CycD1 levels in AD-NSCs. Further, in Nup153-overexpressing AD-NSCs, the expression of TLX/NR2E1 is also recovered. TLX/NR2E1 is a transcription factor reported as a master regulator of NSC self-renewal, maintenance, and neurogenesis through the control of a broad network of genes [37], and its dysfunction plays a key role in neurological disorders [38]. Thus, the upregulation of two important epigenetic regulators such as Nup153 and TLX/NR2E1 may provide the key mechanism to explain the increased function and responsiveness of AD-NSCs by changing chromatin structure.

Along this line, we found that Nup153 overexpression in AD-NSCs also normalized epigenetic marks such as phosphorylation on serine 10 and acetylation on lysines 9 and 14 on histone H3 suggesting an important effect on chromatin conformation and activation.

We have recently reported that, in different contexts, Nup153 levels and epigenetic function were regulated by nitric oxide/oxidative stress signaling [9, 22]. In the present paper, we report that alteration of ˙NO pathway, oxidative stress, and Aβ accumulation affected Nup153 expression, shedding more light on the downstream mechanisms responsible for defective neurogenesis ongoing in AD mice.

Oxidative/nitrosative stress arising from mitochondrial dysfunction, NOS enzyme uncoupling, and conversion of ˙NO and O_2 in higher oxides such as peroxynitrite characterizes AD and is believed to be involved in both impaired neurogenesis and neurodegeneration [39, 40]. Several reports indicate that Aβ may affect directly or indirectly mitochondrial biochemistry and bioenergetics [19]. Moreover, other evidence indicates that Aβ induces abnormal ˙NO release via extrasynaptic *N*-methyl-D-aspartate receptor (NMDAr) [41], thus contributing to nitrosative stress [42]. In this regard, Dias and colleagues investigated age-related alterations in the NMDAr-˙NO pathway in the hippocampus of 3×Tg AD mice revealing significant changes in NMDAr-associated ˙NO concentration dynamics profile in the AD model from an early age, followed by alterations in energy metabolic status and consistent with a putative shift in ˙NO bioactivity towards oxidative chemistry associated with neurotoxicity [43].

On the other hand, aberrant expression of nNOS and iNOS has been largely documented in the hippocampal region of 3×Tg AD mouse model [44]. Recent reports also describe that NOS inhibition by LNAME (NOS pan-inhibitor) or aminoglycoside (iNOS inhibitor) treatments counteracts memory impairment induced by intrahippocampal injection of Aβ in rats [45, 46]. Based on this evidence and given the important regulatory role of ˙NO in Nup153 function, we explored the possible contribution of Aβ to Nup153 alteration in AD-NSCs. Our data indicate indeed that lowering Aβ accumulation by pharmacological treatment (γ-secretase inhibitor), decreasing ˙NO levels (LNAME treatment), or reducing oxidative species (antioxidant treatments) normalize Nup153 protein levels in AD-NSCs. One possible interpretation is that Aβ accumulation, which occurs early also in NSCs from AD mice, inducing eNOS/nNOS uncoupling and iNOS activation, may negatively affect Nup153. Conversely, many lines of evidence show that NOS dysfunction and nitro-oxidative stress also lead to Aβ accumulation [47], thus suggesting the existence of a positive feedback loop between ˙NO dysfunction and Aβ generation which may promote and sustain AD development [48] through Nup153 dysfunction. More importantly, Nup153 expression is recovered after ascorbate treatment. Indeed, ascorbate is a well-known antioxidant which regulates energy metabolism and signaling in the brain and its reduction during aging is associated with cognitive decline and AD. An activity-dependent coupling between ˙NO and ascorbate in the brain has been reported [49] further supporting the implication of ˙NO and oxidative stress pathways in Nup153 regulation.

Conclusions

Overall, our work provides new insights in the molecular pathways that are affected in AD-NSCs. Indeed, alteration in ˙NO balance and nitrosative stress, ongoing in AD pathology, affects the function of Nup153 implicated in the regulation of NSC fate. Importantly, Nup153 reduction was found in NSCs isolated from newborn mice and in the hippocampal niche of young AD mice, before the formation of Aβ plaques and cognitive decline, thus suggesting that Nup153 dysfunction is an early event in AD. Restoration of Nup153 levels in AD-NSCs recovered their proliferative and differentiative capabilities. Further in vivo studies will be required to confirm the role of Nup153 in defective adult neurogenesis in AD and to validate this protein as possible target to boost endogenous neurogenesis and counteract cognitive decline.

Acknowledgements We thank Professor D. Puzzo, from University of Catania, who kindly provided tissues from APP knock-out mice (*B6.129S7-App^{tm1Dbo}/J*; 4 months old) that were used as negative control in Western blot experiments.

Authors' Contributions Electrophysiology: MD, VL; RT-qPCR: KG, LL, SF; ChIP: SF; NSC experiments and analysis: LL, KG, CC; confocal analysis: CC; WB and IP: CC, DDLP; conceptualization: LL, CC, CG; writing: LL, CC, CG. All authors read and approved the final manuscript.

Availability of Data and Materials All data generated or analyzed during this study are included in this published article and in the additional files.

Compliance with Ethical Standards

Mice were used in agreement with the guidelines of the European Parliament (Directive 2010/63/EU for the protection of laboratory animals) and with the guidelines of the Italian National Institute of Health and were approved by the Institutional Animal Care of Università Cattolica (approval number: 553/2016PR, Rome, Italy).

Competing Interests The authors declare that they have no competing interests.

Abbreviations *AD*, Alzheimer's disease; *Nup153*, nucleoporin153; *NSCs*, neural stem cells; *NO*, nitric oxide; *NAC*, *N*-acetylcysteine; *AA*, ascorbic acid; *LNAME*, L-NG-nitro-arginine methyl ester; *GSI*, γ-secretase inhibitor; *MFI*, mean fluorescence intensity; *TLX/NR2E1*, nuclear receptor subfamily 2 group E member 1

References

1. Braun SM, Jessberger S (2014) Adult neurogenesis: mechanisms and functional significance. Development 141(10):1983–1986. https://doi.org/10.1242/dev.104596
2. Toda T, Gage FH (2017) Review: adult neurogenesis contributes to hippocampal plasticity. Cell Tissue Res 373:693–709. https://doi.org/10.1007/s00441-017-2735-4
3. Caselli RJ, Beach TG, Yaari R, Reiman EM (2006) Alzheimer's disease a century later. J Clin Psychiatry 67(11):1784–1800
4. Hamilton LK, Aumont A, Julien C, Vadnais A, Calon F, Fernandes KJ (2010) Widespread deficits in adult neurogenesis precede plaque and tangle formation in the 3xTg mouse model of Alzheimer's disease. Eur J Neurosci 32(6):905–920. https://doi.org/10.1111/j.1460-9568.2010.07379.x
5. Lazarov O, Hollands C (2016) Hippocampal neurogenesis: learning to remember. Prog Neurobiol 138-140:1–18. https://doi.org/10.1016/j.pneurobio.2015.12.006
6. Fitzsimons CP, van Bodegraven E, Schouten M, Lardenoije R, Kompotis K, Kenis G, van den Hurk M, Boks MP et al (2014) Epigenetic regulation of adult neural stem cells: implications for Alzheimer's disease. Mol Neurodegener 9:25. https://doi.org/10.1186/1750-1326-9-25
7. Raices M, D'Angelo MA (2017) Nuclear pore complexes and regulation of gene expression. Curr Opin Cell Biol 46:26–32. https://doi.org/10.1016/j.ceb.2016.12.006
8. Palancade B, Doye V (2008) Sumoylating and desumoylating enzymes at nuclear pores: underpinning their unexpected duties? Trends Cell Biol 18(4):174–183. https://doi.org/10.1016/j.tcb.2008.02.001
9. Nanni S, Re A, Ripoli C, Gowran A, Nigro P, D'Amario D, Amodeo A, Crea F et al (2016) The nuclear pore protein Nup153 associates with chromatin and regulates cardiac gene expression in dystrophic mdx hearts. Cardiovasc Res 112(2):555–567. https://doi.org/10.1093/cvr/cvw204
10. Re A, Colussi C, Nanni S, Aiello A, Bacci L, Grassi C, Pontecorvi A, Farsetti A (2018) Nucleoporin 153 regulates estrogen-dependent nuclear translocation of endothelial nitric oxide synthase and estrogen receptor beta in prostate cancer. Oncotarget 9(46):27985–27997. https://doi.org/10.18632/oncotarget.25462
11. Jacinto FV, Benner C, Hetzer MW (2015) The nucleoporin Nup153 regulates embryonic stem cell pluripotency through gene silencing. Genes Dev 29(12):1224–1238. https://doi.org/10.1101/gad.260919.115
12. Toda T, Hsu JY, Linker SB, Hu L, Schafer ST, Mertens J, Jacinto FV, Hetzer MW et al (2017) Nup153 interacts with Sox2 to enable bimodal gene regulation and maintenance of neural progenitor cells. Cell Stem Cell 21:618–634.e7. https://doi.org/10.1016/j.stem.2017.08.012
13. Liu GH, Li M, Qu J, Izpisua Belmonte JC (2012) Gating neural development and aging via nuclear pores. Cell Res 22(8):1212–1214. https://doi.org/10.1038/cr.2012.35
14. Zhang J, Snyder SH (1995) Nitric oxide in the nervous system. Annu Rev Pharmacol Toxicol 35:213–233. https://doi.org/10.1146/annurev.pa.35.040195.001241
15. Podda MV, Marcocci ME, Oggiano L, D'Ascenzo M, Tolu E, Palamara AT, Azzena GB, Grassi C (2004) Nitric oxide increases the spontaneous firing rate of rat medial vestibular nucleus neurons in vitro via a cyclic GMP-mediated PKG-independent mechanism. Eur J Neurosci 20(8):2124–2132. https://doi.org/10.1111/j.1460-9568.2004.03674.x
16. Licht T, Keshet E (2015) The vascular niche in adult neurogenesis. Mech Dev 138(Pt 1):56–62. https://doi.org/10.1016/j.mod.2015.06.001
17. Uehara T, Nakamura T, Yao D, Shi ZQ, Gu Z, Ma Y, Masliah E, Nomura Y et al (2006) S-nitrosylated protein-disulphide isomerase links protein misfolding to neurodegeneration. Nature 441(7092):513–517. https://doi.org/10.1038/nature04782
18. He P, Shen Y (2009) Interruption of beta-catenin signaling reduces neurogenesis in Alzheimer's disease. J Neurosci 29(20):6545–6557. https://doi.org/10.1523/JNEUROSCI.0421-09.2009
19. Pajak B, Kania E, Orzechowski A (2016) Killing me softly: connotations to unfolded protein response and oxidative stress in Alzheimer's disease. Oxidative Med Cell Longev 2016:1805304–1805317. https://doi.org/10.1155/2016/1805304
20. Nott A, Watson PM, Robinson JD, Crepaldi L, Riccio A (2008) S-Nitrosylation of histone deacetylase 2 induces chromatin remodelling in neurons. Nature 455(7211):411–415. https://doi.org/10.1038/nature07238
21. Colussi C, Mozzetta C, Gurtner A, Illi B, Rosati J, Straino S, Ragone G, Pescatori M et al (2008) HDAC2 blockade by nitric oxide and histone deacetylase inhibitors reveals a common target in Duchenne muscular dystrophy treatment. Proc Natl Acad Sci U S A 105(49):19183–19187. https://doi.org/10.1073/pnas.0805514105
22. Re A, Colussi C, Nanni S, Aiello A, Bacci L, Grassi C, Pontecorvi A, Farsetti A (2018) Nucleoporin 153 regulates estrogen dependent nuclear translocation of endothelial nitric oxide synthase and estrogen receptor beta in prostate cancer. Oncotarget 9(46):27985–27997
23. Kodiha M, Chu A, Matusiewicz N, Stochaj U (2004) Multiple mechanisms promote the inhibition of classical nuclear import upon exposure to severe oxidative stress. Cell Death Differ 11(8):862–874. https://doi.org/10.1038/sj.cdd.4401432
24. Kodiha M, Tran D, Qian C, Morogan A, Presley JF, Brown CM, Stochaj U (2008) Oxidative stress mislocalizes and retains transport factor importin-alpha and nucleoporins Nup153 and Nup88 in nuclei where they generate high molecular mass complexes. Biochim Biophys Acta 1783(3):405–418. https://doi.org/10.1016/j.bbamcr.2007.10.022
25. Mastrodonato A, Barbati SA, Leone L, Colussi C, Gironi K, Rinaudo M, Piacentini R, Denny CA et al (2018) Olfactory memory is enhanced in mice exposed to extremely low-frequency electromagnetic fields via Wnt/beta-catenin dependent modulation of subventricular zone neurogenesis. Sci Rep 8(1):262. https://doi.org/10.1038/s41598-017-18676-1
26. Puzzo D, Piacentini R, Fa M, Gulisano W, Li Puma DD, Staniszewski A, Zhang H, Tropea MR et al (2017) LTP and memory impairment caused by extracellular Abeta and Tau oligomers is APP-dependent. Elife 6. https://doi.org/10.7554/eLife.26991
27. Nanni S, Aiello A, Re A, Guffanti A, Benvenuti V, Colussi C, Castro-Vega LJ, Felsani A et al (2013) Estrogen-dependent dynamic profile of eNOS-DNA associations in prostate cancer. PLoS One 8(5):e62522. https://doi.org/10.1371/journal.pone.0062522
28. Nanni S, Benvenuti V, Grasselli A, Priolo C, Aiello A, Mattiussi S, Colussi C, Lirangi V et al (2009) Endothelial NOS, estrogen receptor beta, and HIFs cooperate in the activation of a prognostic transcriptional pattern in aggressive human prostate cancer. J Clin Invest 119(5):1093–1108. https://doi.org/10.1172/JCI35079
29. Re A, Aiello A, Nanni S, Grasselli A, Benvenuti V, Pantisano V, Strigari L, Colussi C et al (2011) Silencing of GSTP1, a prostate cancer prognostic gene, by the estrogen receptor-beta and endothelial nitric oxide synthase complex. Mol Endocrinol 25(12):2003–2016. https://doi.org/10.1210/me.2011-1024
30. Spinelli M, Fusco S, Mainardi M, Scala F, Natale F, Lapenta R, Mattera A, Rinaudo M et al (2017) Brain insulin resistance impairs hippocampal synaptic plasticity and memory by increasing GluA1 palmitoylation through FoxO3a. Nat Commun 8(1):2009. https://doi.org/10.1038/s41467-017-02221-9

31. Aceto G, Re A, Mattera A, Leone L, Colussi C, Rinaudo M, Scala F, Gironi K et al (2018) GSK3beta modulates timing-dependent long-term depression through direct phosphorylation of Kv4.2 channels. Cereb Cortex. https://doi.org/10.1093/cercor/bhy042
32. Biella G, Di Febo F, Goffredo D, Moiana A, Taglietti V, Conti L, Cattaneo E, Toselli M (2007) Differentiating embryonic stem-derived neural stem cells show a maturation-dependent pattern of voltage-gated sodium current expression and graded action potentials. Neuroscience 149(1):38–52. https://doi.org/10.1016/j.neuroscience.2007.07.021
33. Haughey NJ, Liu D, Nath A, Borchard AC, Mattson MP (2002) Disruption of neurogenesis in the subventricular zone of adult mice, and in human cortical neuronal precursor cells in culture, by amyloid beta-peptide: implications for the pathogenesis of Alzheimer's disease. NeuroMolecular Med 1(2):125–135. https://doi.org/10.1385/NMM:1:2:125
34. Lugert S, Basak O, Knuckles P, Haussler U, Fabel K, Gotz M, Haas CA, Kempermann G et al (2010) Quiescent and active hippocampal neural stem cells with distinct morphologies respond selectively to physiological and pathological stimuli and aging. Cell Stem Cell 6(5):445–456. https://doi.org/10.1016/j.stem.2010.03.017
35. Hagey DW, Muhr J (2014) Sox2 acts in a dose-dependent fashion to regulate proliferation of cortical progenitors. Cell Rep 9(5):1908–1920. https://doi.org/10.1016/j.celrep.2014.11.013
36. Schmid RS, Maness PF (2008) L1 and NCAM adhesion molecules as signaling coreceptors in neuronal migration and process outgrowth. Curr Opin Neurobiol 18(3):245–250. https://doi.org/10.1016/j.conb.2008.07.015
37. Islam MM, Zhang CL (2015) TLX: a master regulator for neural stem cell maintenance and neurogenesis. Biochim Biophys Acta 1849(2):210–216. https://doi.org/10.1016/j.bbagrm.2014.06.001
38. Sun G, Cui Q, Shi Y (2017) Nuclear receptor TLX in development and diseases. Curr Top Dev Biol 125:257–273. https://doi.org/10.1016/bs.ctdb.2016.12.003
39. Serini S, Calviello G (2016) Reduction of oxidative/nitrosative stress in brain and its involvement in the neuroprotective effect of n-3 PUFA in Alzheimer's disease. Curr Alzheimer Res 13(2):123–134
40. Swomley AM, Butterfield DA (2015) Oxidative stress in Alzheimer disease and mild cognitive impairment: evidence from human data provided by redox proteomics. Arch Toxicol 89(10):1669–1680. https://doi.org/10.1007/s00204-015-1556-z
41. Molokanova E, Akhtar MW, Sanz-Blasco S, Tu S, Pina-Crespo JC, McKercher SR, Lipton SA (2014) Differential effects of synaptic and extrasynaptic NMDA receptors on Abeta-induced nitric oxide production in cerebrocortical neurons. J Neurosci 34(14):5023–5028. https://doi.org/10.1523/JNEUROSCI.2907-13.2014
42. Tajes M, Eraso-Pichot A, Rubio-Moscardo F, Guivernau B, Ramos-Fernandez E, Bosch-Morato M, Guix FX, Clarimon J et al (2014) Methylglyoxal produced by amyloid-beta peptide-induced nitrotyrosination of triosephosphate isomerase triggers neuronal death in Alzheimer's disease. J Alzheimers Dis 41(1):273–288. https://doi.org/10.3233/JAD-131685
43. Dias C, Lourenco CF, Ferreiro E, Barbosa RM, Laranjinha J, Ledo A (2016) Age-dependent changes in the glutamate-nitric oxide pathway in the hippocampus of the triple transgenic model of Alzheimer's disease: implications for neurometabolic regulation. Neurobiol Aging 46:84–95. https://doi.org/10.1016/j.neurobiolaging.2016.06.012
44. Lourenco CF, Ledo A, Barbosa RM, Laranjinha J (2017) Neurovascular uncoupling in the triple transgenic model of Alzheimer's disease: impaired cerebral blood flow response to neuronal-derived nitric oxide signaling. Exp Neurol 291:36–43. https://doi.org/10.1016/j.expneurol.2017.01.013
45. Shariatpanahi M, Khodagholi F, Ashabi G, Aghazadeh Khasraghi A, Azimi L, Abdollahi M, Ghahremani MH, Ostad SN et al (2015) Ameliorating of memory impairment and apoptosis in amyloid beta-injected rats via inhibition of nitric oxide synthase: possible participation of autophagy. Iran J Pharm Res 14(3):811–824
46. Diaz A, Rojas K, Espinosa B, Chavez R, Zenteno E, Limon D, Guevara J (2014) Aminoguanidine treatment ameliorates inflammatory responses and memory impairment induced by amyloid-beta 25-35 injection in rats. Neuropeptides 48(3):153–159. https://doi.org/10.1016/j.npep.2014.03.002
47. Austin SA, Santhanam AV, Hinton DJ, Choi DS, Katusic ZS (2013) Endothelial nitric oxide deficiency promotes Alzheimer's disease pathology. J Neurochem 127(5):691–700. https://doi.org/10.1111/jnc.12334
48. Nagai N, Ito Y, Shibata T, Kubo E, Sasaki H (2017) A positive feedback loop between nitric oxide and amyloid beta (1-42) accelerates mitochondrial damage in human lens epithelial cells. Toxicology 381:19–30. https://doi.org/10.1016/j.tox.2017.02.014
49. Ferreira NR, Ledo A, Laranjinha J, Gerhardt GA, Barbosa RM (2018) Simultaneous measurements of ascorbate and glutamate in vivo in the rat brain using carbon fiber nanocomposite sensors and microbiosensor arrays. Bioelectrochemistry 121:142–150. https://doi.org/10.1016/j.bioelechem.2018.01.009